

Fuzzy Dark Matter as a Solution to Reconcile the Stellar Mass Density of High- z Galaxies and Reionization History

YAN GONG,¹ BIN YUE,¹ YE CAO,^{2,3} AND XUELEI CHEN^{1,4,5,6}

¹*National Astronomical Observatories, Chinese Academy of Sciences, Beijing 100101, China*

²*Institute for Frontier in Astronomy and Astrophysics, Beijing Normal University, Beijing, 102206, China*

³*Department of Astronomy, Beijing Normal University, Beijing 100875, China*

⁴*University of Chinese Academy of Sciences, Beijing 100049, China*

⁵*Department of Physics, College of Sciences, Northeastern University, Shenyang 110819, China*

⁶*Center for High Energy Physics, Peking University, Beijing 100871, China*

ABSTRACT

The *JWST* early release data show unexpected high stellar mass densities of massive galaxies at $7 < z < 11$, a high star formation efficiency is probably needed to explain this. However, such a high star formation efficiency would greatly increase the number of ionizing photons, which would be in serious conflict with current cosmic microwave background (CMB) and other measurements of cosmic reionization history. To solve this problem, we explore the fuzzy dark matter (FDM), which is composed of ultra-light scalar particles, e.g. ultra-light axions, and calculate its halo mass function and stellar mass density for different axion masses. We find that the FDM model with $m_a \simeq 5 \times 10^{-23}$ eV and an uncertainty range of $3 \times 10^{-23} - 10^{-22}$ eV can effectively suppress the formation of small halos and galaxies, so that with higher star formation efficiency, both the *JWST* data at $z \sim 8$ and the reionization history measurements from optical depth of CMB scattering and ionization fraction can be simultaneously matched. We also find that the *JWST* data at $z \sim 10$ are still too high to fit in this scenario. We note that the estimated mean redshift of the sample may have large uncertainty, that it can be as low as $z \sim 9$ depending on adopted spectral energy distribution (SED) templates and photometric-redshift code. Besides, the warm dark matter with \sim keV mass can also be an alternative choice, since it should have similar effects on halo formation as the FDM.

Keywords: cosmology:theory-dark matter-large scale structure of universe

1. INTRODUCTION

Exploration of high-redshift (high- z) galaxies can provide valuable information of galaxy formation and history of cosmic reionization. Recently, the *James Webb Space Telescope* (*JWST*) has released early observational results of detecting galaxies at $z \gtrsim 10$, and some unexpected discoveries have been found that may be in tension with the current galaxy formation theory and the widely accepted Λ CDM model as well (Boylan-Kolchin 2022; Lovell et al. 2022; Mason et al. 2022; Menci et al. 2022; Mirocha et al. 2022; Naidu et al. 2022a,b). In particular, Labbe et al. (2022) reported a much higher stellar mass density in massive galaxies with $M_* = 10^{10} - 10^{11} M_\odot$ at $7 < z < 11$, which is more than one magnitude higher at $z \sim 8$, and three orders of magnitude higher at $z \sim 10$, than the anticipated values from the standard cosmology and star formation sce-

narios, raising a challenge to the standard cosmological model.

One way to explain this huge abundance excess is to dramatically enhance the star formation rate (SFR) or UV luminosity function at high- z by invoking a large star formation efficiency f_* , which indicates the fraction of baryons that can convert to stars (Boylan-Kolchin 2022; Lovell et al. 2022; Mason et al. 2022; Mirocha et al. 2022). Although the typical values of f_* is usually expected to be less than 0.1 based on observations at lower redshifts, it is theoretically possible to have a larger value, even up to $f_* \sim 1$ at the high redshifts, as f_* depends on complicated physics of star formation. Adoption of the higher f_* could partially solve or at least reduce the tension between theories and the *JWST* observation. However, this may raise new tension with the cosmic reionization history, which is closely related to high- z star formation process, and is well constrained

by current cosmological observations, such as the cosmic microwave background (CMB) as measured by the *WMAP* and *Planck* satellites (e.g. [Hinshaw et al. 2013](#); [Planck Collaboration et al. 2020](#)). With a higher star formation efficiency, for a given halo mass M , more massive galaxy can be formed, but then there is an overall increase of ionizing photons produced, and the Universe would be reionized much earlier than as inferred from current observations.

As only the more massive galaxies is detectable at high redshifts with the current *JWST* observations, one possible way to resolve this conflict is to boost the formation of massive galaxies while suppress the formation of small galaxies. One can apply a mass-dependent star formation efficiency $f_*(M)$ to suppress the star formation in small halos, but as we shall discuss later, this may still not be enough to explain the observational results.

Here we propose and explore the fuzzy dark matter (FDM) as a solution to this problem. The FDM is a proposed dark matter composed of ultra-light scalar particles ([Hu et al. 2000](#)), such as ultra-light axions (see e.g. [Marsh 2016a](#)). Since the FDM particles have extremely low mass with $m_a \sim 10^{-22}$ eV, its de Broglie wavelength can be as large as the size of a dwarf galaxy or even larger. Due to the uncertainty principle in wave mechanics, an effective quantum pressure arises to suppress matter fluctuations below a certain Jeans scale, so small structures cannot form. This will affect the formation and density profile of objects on small scales, and severely suppress the halo mass function at small masses. If the dark matter is composed of FDM, only relatively large halos and massive galaxies are formed, and the rest of dark matter will not cluster, and stay as a smooth component in linear regime. Therefore, it will not significantly affect cosmic reionization history, even when the star formation efficiency is greatly enhanced at high redshifts, since small galaxies do not form in this model.

A number of observations have been performed for probing the FDM, including measurements of density profile and mass function of dwarf galaxies, rotation curves of Milky Way, Ly α forest that exploring cosmic structures on small scales, and so on ([Schive et al. 2014](#); [Marsh & Niemeyer 2019](#); [Safarzadeh & Spergel 2019](#); [Broadhurst et al. 2020](#); [Irsic et al. 2017](#); [Armen-gaud et al. 2017](#); [Maleki et al. 2020](#)). Possible mass ranges or lower limits of mass of the FDM particles have been derived from these detections. Although some inconsistency may still exist in the current observations, e.g. the observations of Milky Way's dwarf satellites ([Safarzadeh & Spergel 2019](#)), an interesting and possible region around $m_a \sim 10^{-22}$ eV can be located,

which is worth for further study. In the following discussion, we assume a flat Λ CDM model with $\Omega_b = 0.0493$, $\Omega_m = 0.3153$, $h = 0.6736$, $\sigma_8 = 0.8111$, $n_s = 0.9649$ ([Planck Collaboration et al. 2020](#)).

2. MODEL

Since the FDM cannot form small halos below a certain Jeans scale due to quantum pressure, the halo mass function is suppressed at low mass end. The FDM halo mass function has been discussed in previous literatures based on numerical simulations and semi-analytic techniques (see e.g. [Schive et al. 2016](#); [Du et al. 2018](#); [Schutz 2020](#); [Niemeyer 2019](#)). Here we use a mass-dependent critical overdensity $\delta_c(M, z)$ in the analytical mass function to account for this suppression at small mass scale ([Marsh & Silk 2014](#); [Bozek et al. 2015](#); [Marsh 2016b](#); [Du et al. 2017](#)), which is given by

$$\delta_c(M, z) = \mathcal{G}(M) \delta_{\text{crit}}(z). \quad (1)$$

Here $\delta_{\text{crit}}(z) = \delta_{\text{crit}}^0/D(z)$, where $\delta_{\text{crit}}^0 \approx 1.686$ is the critical overdensity for collapse, and $D(z)$ is the linear growth factor normalized at $z = 0$. $\mathcal{G}(M)$ is a factor accounting for mass-dependence, it can be computed with the *AxionCMB* code([Hlozek et al. 2015](#)), and fitted as functions of halo and axion masses (e.g. [Marsh & Silk 2014](#); [Marsh 2016b](#); [Du et al. 2017](#)).

The FDM halo mass function can be obtained with this critical density in the Press-Schechter approach ([Press & Schechter 1974](#)),

$$n(M, z)dM = \frac{\bar{\rho}_m}{M} \nu f(\nu) \frac{d\nu}{\nu}, \quad (2)$$

where $\bar{\rho}_m = \Omega_m \rho_{\text{crit}}$ is the current matter density, ρ_{crit} is the current critical density, and for $\nu f(\nu)$ we take the form as ([Sheth & Tormen 1999](#))

$$\nu f(\nu) = A \sqrt{\frac{\nu'}{2\pi}} (1 + \nu'^{-p}) e^{-\nu'/2}. \quad (3)$$

Here $\nu' = a\nu$, $a = 0.707$, $p = 0.3$, A is the normalization factor, $\nu \equiv [\delta_c(M, z)/\sigma(M)]^2$, and $\sigma^2(M)$ is the variance of linear power spectrum. For the FDM linear matter power spectrum, we adopt a numerical result given by [Hu et al. \(2000\)](#). Considering suppression of the FDM power spectrum relative to the CDM case, we have

$$P_{\text{lin}}^{\text{FDM}}(k, z) = T_{\text{F}}^2(k) P_{\text{lin}}^{\text{CDM}}(k, z). \quad (4)$$

Here $P_{\text{lin}}^{\text{CDM}}$ is the CDM linear power spectrum, which can be estimated analytically ([Eisenstein & Hu 1998](#)). $T_{\text{F}}(k) \approx \cos x^3/(1 + x^8)$ is the transfer function, and $x = 1.61 m_{22}^{1/18} k/k_{\text{J}}^{\text{eq}}$, where $m_{22} = m_a/10^{-22}$ eV and $k_{\text{J}}^{\text{eq}} = 9 m_{22}^{1/2} \text{Mpc}^{-1}$ is the comoving Jeans wavenumber

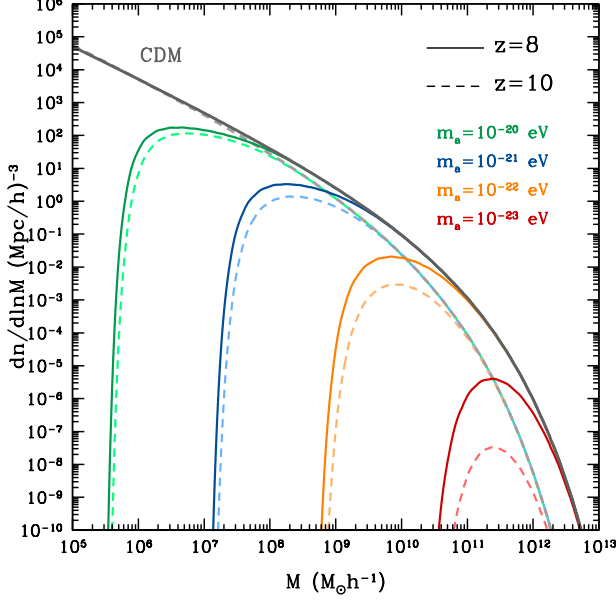


Figure 1. The FDM halo mass functions for different axion masses are shown in solid ($z = 8$) and dashed ($z = 10$) curves. The CDM halo mass functions are also plotted in gray curves for comparison. We can find that small halos with low masses cannot form in FDM.

scale at epoch of matter-radiation equality. The transfer function has acoustic oscillation features on small scales below k_J^{eq} , and will approach to unity for large FDM particle mass when $m_a \gg 10^{-22}$ eV or $m_{22} \gg 1$. The FDM halo mass functions at $z = 8$ (solid) and $z = 10$ (dashed) for different axion masses are shown in Figure 1. We can see that the abundance of low-mass halos is greatly suppressed in FDM, and only massive halos can form with the same mass function as the CDM case. This allows adopting larger number density for massive galaxies without over-producing ionizing photons.

Hence, the comoving cumulative halo mass density with halo mass greater than M can be calculated by

$$\rho(> M, z) = \int_M^\infty dM' M' n(M', z). \quad (5)$$

Considering the relation between the halo mass and stellar mass, i.e. $M_* = f_*(\Omega_b/\Omega_m) M = \epsilon M$, we obtain the cumulative stellar mass density with stellar mass larger than M_* ,

$$\rho_*(> M_*, z) = \epsilon \rho(> M_*/\epsilon, z). \quad (6)$$

We consider two forms of star formation efficiency in this work, i.e. mass-independent $f_* = \text{const}$ and mass-dependent $f_*(M)$, for the latter we assume a double power-law (DPL) form as given in Mirocha et al. (2017)

$$f_*(M) = \frac{2f_*^0}{\left(\frac{M}{M_p}\right)^{\alpha_{\text{lo}}} + \left(\frac{M}{M_p}\right)^{\alpha_{\text{hi}}}}, \quad (7)$$

where we adopt $M_p = 2.8 \times 10^{11} M_\odot$, $\alpha_{\text{lo}} = 0.49$, and $\alpha_{\text{hi}} = -0.61$. These parameters are calibrated to match the observed high- z LFs (Bouwens et al. 2015a). f_*^0 is the star formation efficiency at halo mass M_p , and they find $f_*^0 = 0.025$ ¹. We will adjust f_*^0 and f_* to match the *JWST* data in this work.

As we mentioned, a large star formation efficiency can significantly affect the cosmic reionization history, and may violate the current measurements of epoch of reionization. To evaluate this effect, we can first calculate the hydrogen volume filling factor $Q_{\text{HII}}(z)$ as a function of redshift. The evolution of Q_{HII} follows (Wyith & Loeb 2003; Madau et al. 1999)

$$\frac{dQ_{\text{HII}}}{dt} = f_{\text{esc}} \frac{\dot{n}_{\text{ion}}}{\bar{n}_{\text{H}}} - C_{\text{HII}}(z) \alpha_B(T_{\text{HII}}) \bar{n}_{\text{H}} (1+z)^3 x_e, \quad (8)$$

where f_{esc} is the escape fraction set to be 0.1 (Sun et al. 2021), \bar{n}_{H} is the mean number density of hydrogen (both neutral and ionized) atoms at present Universe, $C_{\text{HII}} = 3.0$ is the clumping factor of the ionized gas (Kaurov & Gendin 2014), α_B is the Case B recombination coefficient, and T_{HII} is the kinetic temperature. We always take $T_{\text{HII}} = 2 \times 10^4$ K (Robertson et al. 2015), so that $\alpha_B = 2.5 \times 10^{-13} \text{ cm}^3 \text{ s}^{-1}$. Here for simplicity we assume the helium has the same first stage ionization (i.e. He II) fraction as hydrogen (the full ionization to He III would be much later), so the total ionization fraction can be written as

$$x_e = Q_{\text{HII}} \left(1 + \frac{Y_{\text{He}}}{4}\right), \quad (9)$$

where $Y_{\text{He}} = 0.25$ is the Helium element abundance. For the emission rate of ionizing photons per unit comoving volume \dot{n}_{ion} , we take

$$\dot{n}_{\text{ion}} = N_{\text{ion}} \frac{\Omega_b}{\Omega_m} \frac{1}{t_{\text{SF}}(z)} \int_{M_{\text{min}}}^\infty dM n(M, z) f_*(M) M, \quad (10)$$

where $N_{\text{ion}} \approx 4000$ is the total ionizing photons produced per stellar baryon throughout its lifetime for typical Pop II galaxies (e.g. see Starburst99², Leitherer et al. 1999; Vazquez & Leitherer 2005; Leitherer et al. 2010, 2014), t_{SF} is the star-forming timescale, and we assume that it equals to 10% of the Hubble time at redshift

¹ Note that there is an additional factor 2 in the numerator compared to that given in Mirocha et al. (2017).

² <https://www.stsci.edu/science/starburst99/docs/default.htm>

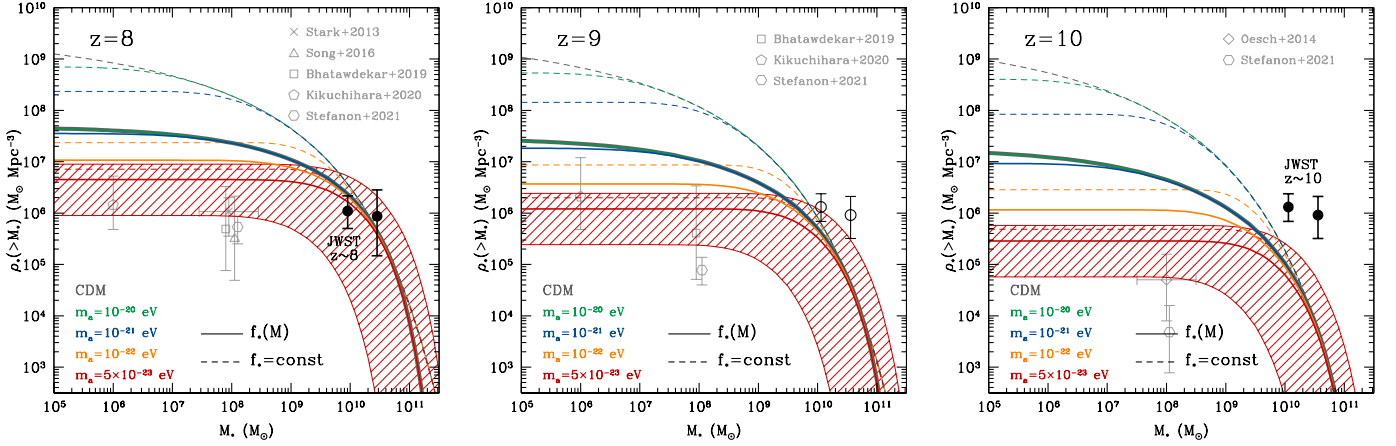


Figure 2. The comoving cumulative stellar mass density as a function of stellar mass for different axion masses at $z = 8$ (left panel), $z = 9$ (middle panel) and $z = 10$ (right panel). The solid curves denote the results derived from the mass-dependent star formation efficiency $f_*(M)$ with $f_*^0 = 0.5$, and the dashed curves are for constant $f_* = 0.5$. The hatched region shows the range of the results of $m_a = 5 \times 10^{-23}$ eV with $f_*^0 = 0.1 - 1$. For comparison, the results of the CDM case are also shown in gray curves. The *JWST* measured values at mean redshift $z \sim 8$ and $z \sim 10$ as given by Labbe et al. (2022) are over-plotted as black solid dots with error bars in the Left and Right panels, respectively. Our estimate shows that the mean redshift for the second group could be $z \sim 9$, so we also plot them as open circles in the Middle panel. The data at low stellar mass are also shown in gray data points for comparison, given by Stark et al. (2013), Oesch et al. (2014), Song et al. (2016), Bhatawdekar et al. (2019), Kikuchihiro et al. (2020), and Stefanon et al. (2021). Note that we assume an intrinsic dispersion of 0.5 dex for the $\log M_{UV} - M_*$ relation when plot the data points given in Stark et al. (2013) and Oesch et al. (2014). To show these data clearly, we make little shifts for the data at $M_* = 10^8 M_\odot$.

z (Wyith & Loeb 2006; Lidz et al. 2011). M_{\min} is the minimum halo mass corresponding to a virial temperature of 10^4 K, halos above this mass can sustain effective cooling via the Ly α transition (Barkana & Loeb 2001). We find that, for example, $M_{\min} = 4.6 \times 10^7$, 8.0×10^7 , and $2.0 \times 10^8 M_\odot$ at $z = 15$, 10, and 5, respectively. The major contribution of ionizing photons depends on the shape of $f_*(M)n(M, z)$, and basically it is dominated by low-mass galaxies in the CDM model. In the FDM model, it can be dominated by massive galaxies, since small galaxies can barely form when m_a is small.

The optical depth of the CMB scattering is adopted as a quantity to characterize the cosmic reionization history, which can be estimated by

$$\tau = \int_0^\infty \sigma_T \bar{n}_H (1+z)^3 x_e \frac{cdz}{(1+z)H(z)}, \quad (11)$$

where $\sigma_T = 6.65 \times 10^{-25} \text{ cm}^2$ is the Thompson scattering cross-section. We integrate up to $z_{\max} = 30$ since the reionization is negligible before this redshift in our model.

3. RESULT

In Figure 2, we show the comoving cumulative stellar mass density $\rho_*(> M_*)$ as a function of M_* at $z = 8$ (Left panel), 9 (Middle panel) and 10 (Right panel) for the FDM and CDM cases. As can be seen, $\rho_*(> M_*)$ is

effectively suppressed at small stellar masses compared to the CDM case, while at the higher mass end the FDM and CDM curves are identical. For example, at $z = 8$, assuming the mass-dependent star formation efficiency with $f_*^0 = 0.5$, we find that $\rho_*(> M_*)$ almost becomes flat when $M_* \lesssim 10^6$, 10^7 , 10^8 , and $10^9 M_\odot$, when $m_a = 10^{-20}$, 10^{-21} , 10^{-22} , and 5×10^{-23} eV, respectively. As expected, this effect is more significant in the mass-dependent $f_*(M)$ case than the constant f_* case, since $f_*(M)$ would become smaller at small M_* . Labbe et al. (2022) has given the estimates in two redshift groups ($z \sim 8$ and $z \sim 10$), and at each redshift for $M_* > 10^{10} M_\odot$ and $M_* > 10^{10.5} M_\odot$. We also over-plotted these estimates in black solid dots in Figure 2.

If we assume the maximum f_* or f_*^0 can reach to 1, i.e. all baryons will convert to stars in the constant f_* case or at M_p in the $f_*(M)$ case, it seems that both CDM and FDM models considered here can match the data measured by *JWST* at $z \sim 8$ (refer to the hatched region in the left panel of Figure 2). However, as we will discuss below, most of them will not be consistent with the measurements of cosmic reionization history.

On the other hand, we can see that at $z \sim 10$ (the Right panel of Figure 2), none of the CDM or FDM model we considered can fit the *JWST* data even assuming f_* or $f_*^0 = 1$, as have been found in studies assuming the Λ CDM model (e.g. Boylan-Kolchin 2022; Menci et

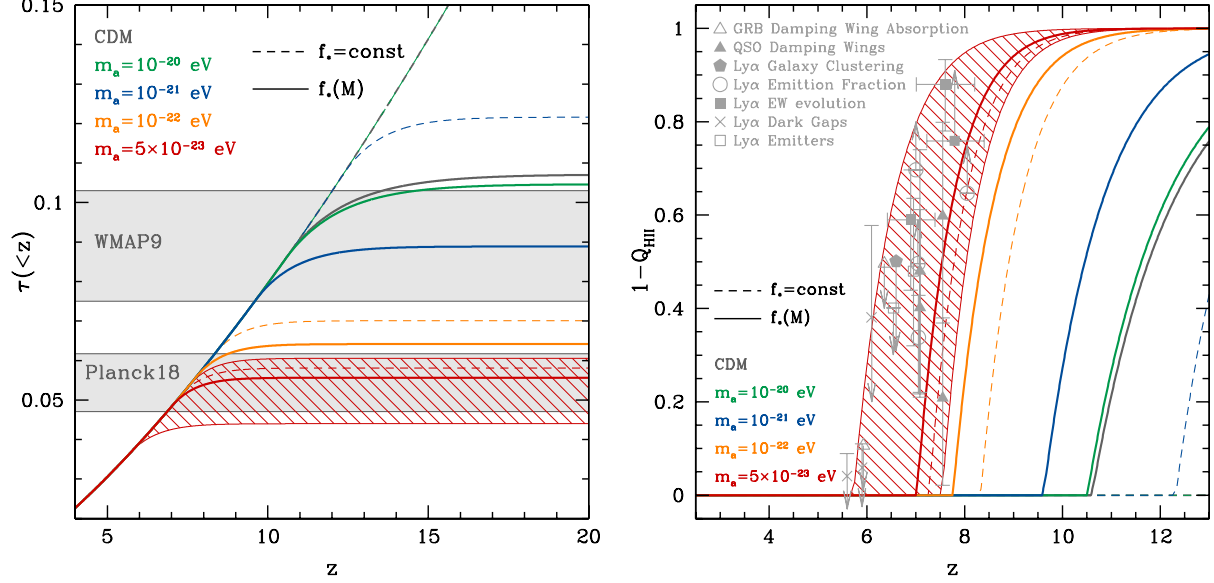


Figure 3. *Left panel:* The optical depth τ as a function of redshift for the FDM and CDM cases. The solid and dashed curves denote the results from mass-dependent $f_*(M)$ with $f_*^0 = 0.5$ and constant $f_* = 0.5$, respectively. The hatched region is for the results derived from $f_*^0 = 0.1 - 1$. The gray shaded regions are the 1σ (68.3% C.L.) results given by WMAP9 (Hinshaw et al. 2013) and Planck18 (Planck Collaboration et al. 2020). *Right panel:* The average IGM neutral hydrogen fraction characterized by $1 - Q_{\text{HII}}$ as a function of redshift. The gray data points show the results of different measurements in previous studies (see e.g. Robertson et al. 2015; Bouwens et al. 2015b; Mason et al. 2019, and the references therein.)

al. 2022). This may be due either to strong deviation of cosmological evolution from the Λ CDM model, or due to issues of galaxy selection, measurements of galaxy stellar mass and redshift, dust extinction, and sample variance (Endsley et al. 2022; Ferrara et al. 2022; Ziparo et al. 2022; Adams et al. 2023).

In particular, the stellar mass and redshift of these galaxies are estimated photometrically in Labbe et al. (2022) using the EAZY code (Brammer et al. 2008). Based on other studies, the stellar mass can be even one order of magnitude lower with different assumptions of SED template fitting (e.g. Endsley et al. 2022), and then $\rho_*(> M_*)$ also will become lower accordingly. If this is true, as shown in Figure 2, the tension between the JWST data and the CDM model with small $f_*^0 < 0.1$ can be relaxed at $z \sim 8$. However, even so the JWST data at $z \sim 10$ seem still too high for the CDM model, although they can match our FDM model with large $f_*^0 > 0.1$ (red hatched region). In addition, the photometric redshift estimation may also have larger errors, especially at these very high redshifts (Adams et al. 2023). To make a simple and practical assessment of this uncertainty, we use another widely used photo- z code, i.e. LePhare (Arnouts et al. 1999; Ilbert et al. 2006), to derive the photometric redshifts of the seven galaxies given in Labbe et al. (2022). A quick check shows that the mean photo- z of the three galaxies in

$7 < z < 9$ and the four galaxies in $9 < z < 11$ are $\bar{z}_p = 8.6 \pm 0.3$ and $9.4^{+0.6}_{-0.4}$, respectively, compared to $\bar{z}_p = 8.3$ and 10.0 given by Labbe et al. (2022). This indicates that there could be relatively large uncertainty in the current galaxy redshift estimation, which depends on the selected photo- z analysis code and spectral energy distribution (SED) templates. If we shift the density mean redshift from $z \sim 10$ to $z \sim 9$, as shown in the Middle panel of Figure 2, the data could be explained by the current models within 1σ error.

Besides, for comparison, we also show the data of stellar mass density at low stellar mass end down to $M_* \sim 10^6$ and $10^8 M_\odot$, which are given by previous studies (Stark et al. 2013; Oesch et al. 2014; Song et al. 2016; Bhatawdekar et al. 2019; Kikuchi et al. 2020; Stefanon et al. 2021). We can see that, our model with $m_a = 5 \times 10^{-23}$ eV and $f_*^0 = 0.1 - 1$ (red hatched region) is consistent with most of these data within 1σ confidence level. This means that our FDM model is able to explain both the measurement of stellar mass density from JWST at high stellar mass and the data obtained at low stellar mass. On the other hand, it seems that the CDM model can hardly fit all these data in the mean time, no matter assuming large or small star formation efficiency.

In the left panel of Figure 3, we plot the optical depth τ as a function of z for the CDM and FDM models.

The 68.3% confidence level (C.L.) results of the 9-year *WMAP* (WMAP9) and *Planck* 2018 (Planck18) (Hinshaw et al. 2013; Planck Collaboration et al. 2020) are also shown in gray parallel bands, which give $\tau = 0.089 \pm 0.014$ and 0.0540 ± 0.0074 , respectively. Note that the WMAP9 result is actually consistent with *Planck* 2015 result with $\tau = 0.079 \pm 0.017$ (Planck Collaboration et al. 2016) in 1σ error. We can find that the case of $m_a = 5 \times 10^{-23}$ eV can fit the Planck18 result very well for both mass-dependent and constant star formation efficiencies, and the $m_a = 10^{-21}$ eV case is consistent with the WMAP9 results for mass-dependent $f_*(M)$. Both the CDM cases of assuming mass-dependent $f_*(M)$ with $f_*^0 = 0.5$ and constant $f_* = 0.5$ (gray curves) predict much higher τ , that cannot fit the measurements. Hence, although most of these FDM and CDM models can fit the *JWST* data at $z \sim 8$ (see the left panel of Figure 2), only $m_a = 5 \times 10^{-23}$ and 10^{-21} eV can give good match to the cosmic reionization history measured by *Planck* and *WMAP* satellites, respectively.

In addition, we show the neutral hydrogen fraction of the intergalactic medium (IGM) characterized by $1 - Q_{\text{HII}}$ as a function of redshift in the right panel of Figure 3. The results from Ly α galaxies, gamma-ray burst (GRB), and quasi-stellar object (QSO) measurements are shown in gray data points (see e.g. Robertson et al. 2015; Bouwens et al. 2015b; Mason et al. 2019). We can see that the FDM model with $m_a = 5 \times 10^{-23}$ and $f_*^0 = 0.1 - 1$ (red hatched region) are in good agreement with these data, and the models with other axion masses cannot fit the data very well. Hence, it indicates that the FDM model with $m_a = 5 \times 10^{-23}$ can match all the data of high- z galaxy stellar mass density and reionization history measured by optical depth and IGM neutral hydrogen fraction. We also should note that there are large uncertainties in the current analytical estimation, such as star formation efficiency, escape fraction, clumping factor and so on (Finkelstein et al. 2019; Yung et al. 2020), so the axion mass we derive also has an uncertainty range. Considering the uncertainties of the terms in the model and the errors of the data we consider, a possible m_a range of $3 \times 10^{-23} - 10^{-22}$ eV can be obtained.

4. CONCLUSION

We explore the FDM as a solution to reconcile the unexpected high stellar mass density of massive galaxies at $7 < z < 11$ obtained in the *JWST* early release measurements and the reionization history. To explain this high density, a large star formation efficiency is probably needed, which may greatly boost the number of ionizing photons and violate the cosmic reionization history measured by current CMB and other observations. The FDM that is composed of ultra-light scalar particles, e.g. ultra-light axions, can effectively suppress the formation of small halos and galaxies due to the galaxy-size de Broglie wavelength. This provides a possible way to solve this problem.

By exploring the FDM with different axion masses, we find that the FDM model can simultaneously fit the cumulative stellar mass density data from the *JWST* at $z \sim 8$ and the optical depth of the CMB scattering τ , when the axion mass $m_a \simeq 5 \times 10^{-23}$ and 10^{-21} eV for the Planck18 and WMAP9 results, respectively. After considering the reionization history measurements by the IGM ionization fraction Q_{HII} , only $m_a \simeq 5 \times 10^{-23}$ is preferred. Although the *JWST* data at $z \sim 10$ are still too high to explain, we find that the current photo- z estimation may have large uncertainties, and the mean redshift of the sample can be as low as $z \sim 9$ if using different SED templates and photo- z codes. Besides, other terms, such as galaxy selection, uncertainty of stellar mass, dust extinction and sample variance, can also affect the results, which needs more data and further studies. With the current uncertainties considered, we find that m_a should be in a range from $\sim 3 \times 10^{-23}$ to $\sim 10^{-22}$ eV to explain the current measurements. We also notice that, in addition to the FDM, the warm dark matter with $\sim \text{keV}$ mass could have similar effect on halo formation as the FDM, and should be worth to investigate in the future work.

1 We acknowledge the support of MOST-
2 2018YFE0120800, 2020SKA0110402, National Key
3 R&D Program of China No.2022YFF0503404, NSFC-
4 11822305, NSFC-11773031, and NSFC-11633004, the
5 Chinese Academy of Science grants QYZDJ-SSW-
6 SLH017, XDB 23040100, XDA15020200. This work
7 is also supported by the science research grants from
8 the China Manned Space Project with NO.CMS-CSST-
9 2021-B01 and CMS- CSST-2021-A01.

REFERENCES

- Adams, N. J., Conselice, C. J., Ferreira, L., et al. 2023, *MNRAS*, 518, 4755-4766
- Armengaud, E., Palanque-Delabrouille, N., Yèche, C., Marsh D. J. E., & Baur, J. 2017, *MNRAS*, 471, 4606-4614

- Arnouts S., Cristiani S., Moscardini L., Matarrese S., Lucchin F., Fontana A., Giallongo E., 1999, *MNRAS*, 310, 540
- Barkana, R., Loeb, A. 2001, *PhR*, 349, 125-238
- Bhatawdekar, R., Conselice, C., Margalef-Bentabol, B., & Duncan, K. 2019, *MNRAS*, 486, 3805
- Bouwens, R. J., Illingworth, G. D., Oesch, P. A., et al. 2015, *ApJ*, 803, 34
- Bouwens, R. J., Illingworth, G. D., Oesch, P. A., et al. 2015, *ApJ*, 811, 140
- Boylan-Kolchin, M. 2022, *arXiv:2208.01611*
- Bozek, B., Marsh, D. J. E., Silk, J., & Wyse, R. F. G. 2015, *MNRAS*, 450, 209-222
- Broadhurst, T., de Martino, I., Luu, H. N., Smoot, G. F., Tye, S. -H. H. 2020, *PRD*, 101, 083012
- Brammer, G. B., van Dokkum, P. G. & Coppi, P. 2008, *ApJ* 686, 1503-1513
- Cooray A., & Sheth, R. 2002, *Phys. Rep.*, 372, 1
- Du, X., Behrens C., & Niemeyer, J. C. 2017, *MNRAS*, 465, 941-951
- Du, X., Schwabe, B., Niemeyer, J. C., & Burger, D. 2018, *PRD*, 97, 063507
- Eisenstein, D. J., & Hu, W. 1998, *ApJ*, 496, 605
- Endsley, R., Stark, D. P., Whitler, L., et al. 2022, *arXiv:2208.14999*
- Ferrara, A., Pallottini, A., & Dayal, P. 2022, *arXiv:2208.00720*
- Finkelstein, S. L., D'Aloisio, A., Paardekooper, J.-P., et al. 2019, *ApJ*, 879, 36
- Hinshaw, G., Larson, D., Komatsu, E., et al. 2013, *ApJS*, 208, 19
- Hlozek, R., Grin, D., Marsh, D. J. E., & Ferreira, P. G. 2015, *PRD*, 91, 103512
- Hu, W., Barkana, R., & Gruzinov, A. 2000, *PRL*, 85, 1158
- Ilbert O. et al., 2006, *A&A*, 457, 841
- Irsic, V., Viel, M., Haehnelt, M. G., Bolton J. S., & Becker, G. D., 2017, *PRL*, 119, 031302
- Kaurov, A. A., & Gnedin, N. Y. 2015, *ApJ*, 810, 154
- Kikuchihara, S., Ouchi, M., Ono, Y., et al. 2020, *ApJ*, 893, 60
- Labbe I. et al., 2022, *arXiv:2207.12446*
- Leitherer, C., Schaerer, D., Goldader, J. D. et al., 1999, *ApJS*, 123, 3-40
- Leitherer, C., et al. 2010, *ApJS*, 189, 309-335
- Leitherer, C., Ekstrom, S., Meynet, G. et al., 2014, *ApJS*, 212, 14
- Lidz, A., Furlanetto, S. R., Oh, S., P., et al. 2011, *ApJ*, 741, 70
- Lovell, C. C., Harrison, I., Harikane, Y., Tacchella, S., Wilkins, S. M. 2022, *arXiv:2208.10479*
- Maleki, A., Baghran S., & Rahvar, S. 2020, *arXiv:2001.04454*
- Madau P., Haardt F., Rees M. J., 1999, *ApJ*, 514, 648
- Marsh, D. J. E., & Silk, J. 2014, *MNRAS*, 437, 2652-2663
- Marsh, D. J. E. 2016, *Phys. Rep.*, 643, 1
- Marsh, D. J. E. 2016, *arXiv:1605.05973*
- Marsh, D. J. E., & Niemeyer, J. C., 2019, *PRL*, 123, 051103
- Mason, C. A., Naidu, R. P., Tacchella, S., & Leja, J. 2019, *MNRAS*, 489, 2669-2676
- Mason, C. A., Trenti, M., Treu, T., et al. 2022, *arXiv:2207.14808*
- Menci, N., Castellano, M., Santini, P., et al. 2022, *arXiv:2208.11471*
- Mirocha, J., Furlanetto, S. R., Sun, G. 2017, *MNRAS*, 464, 1365-1379
- Mirocha, J., & Furlanetto, S. R. 2022, *arXiv:2208.12826*
- Naidu, R. P., Oesch, P., A., van Dokkum, P., et al. 2022, *arXiv:2207.09434*
- Naidu, R. P., Oesch, P., A., Setton, D. J., et al. 2022, *arXiv:2208.02794*
- Niemeyer, J. C. 2019, *arXiv:1912.07064*
- Oesch, P. A., Bouwens, R. J., Illingworth, G. D., et al. 2014, *ApJ*, 786, 108
- Planck Collaboration et al., 2016, *A&A*, 594, A13
- Planck Collaboration et al., 2020, *A&A*, 641, A6
- Press, W. H., & Schechter, P. 1974, *ApJ*, 187, 425
- Robertson, B. E., Ellis, R. S., Furlanetto, S. R., Dunlop, J. S. 2015, *ApJL*, 802, L19
- Safarzadeh, M., & Spergel, D. N. 2019, *arXiv:1906.11848*
- Schive, H.-Y., Chiueh, T., Broadhurst, T. 2014a, *Nature Phys.*, 10, 496
- Schive, H.-Y., Chiueh, T., Broadhurst, T., & Huang, K.-W. 2016, *ApJ*, 818, 89
- Schutz, K. 2020, *arXiv:2001.05503*
- Sheth, R. K., & Tormen, G. 1999, *MNRAS*, 308, 119
- Song, M., Finkelstein, S. L., Ashby, M. L. N., et al. 2016, *ApJ*, 825, 5
- Stark, D. P., Schenker, M. A., Ellis, R., et al. 2013, *ApJ*, 763, 129
- Stefanon, M., Bouwens, R., J., Labbe, I., et al. 2021, *ApJ*, 922, 29
- Sun, G., Mirocha, J., Mebane, R. H., Furlanetto, S. R. 2021, *MNRAS*, 508, 1954-1972
- Vazquez, G. A., & Leitherer, C. 2005, *ApJ*, 621, 695-717
- Wyithe, J. S. B., & Loeb, A. 2003, *ApJ*, 588, L69-L72.
- Wyithe, J. S. B., & Loeb, A. 2006, *Nature*, 441, 322-324
- Yung, L. Y., Somerville, R. S., Finkelstein, S. L., et al. 2020, *MNRAS*, 496, 4574-4592
- Ziparo, F., Ferrara, A., Sommovigo, L., & Kohandel, M. 2022, *arXiv:2209.06840*